Research Article

In-Depth Study of Mass Transfer in Nanoporous Materials by Micro-Imaging

Florian Hibbe[1], Jasper M. van Baten[2], Rajamani Krishna[2], Christian Chmelik[1,*], Jens Weitkamp[3], and Jörg Kärger[1]

DOI: 10.1002/cite.201100167

Dedicated to Prof. Dr. Jürgen Caro on the occasion of his 60th birthday

The first application of interference microscopy to monitoring mass transfer in nanoporous materials dates back to late 1970s when Caro and colleagues reported results of investigations of water uptake by LTA type zeolites. It was, however, not before the beginning of the new millennium that the developments in both the measuring technique and computational power have enabled the recording of transient guest profiles during molecular uptake and release under well-defined conditions, leading to the establishment of a novel access to diffusion studies, now referred to as micro-imaging. In the present contribution, the thus accessible novel type of information is illustrated by an in-depth analysis of the uptake kinetics of methanol in an all-silica ferrierite. In particular, two remarkable experimental findings are reported, which may be tracked back to their microstructural and/or microdynamic origin, namely a pronounced asymmetry in the transient concentration profiles and a slowing down of guest uptake with increasing temperature.

Keywords: Diffusion, Ferrierite, Interference microscopy, Surface permeation, Zeolites

Received: September 06, 2011; *accepted:* September 30, 2011

1 Introduction

Guest diffusion in nanoporous host materials is among the rate-limiting processes in their technological application for upgrading by heterogeneous catalysis, selective adsorption and membrane separation [1–4]. Thus, mass transfer in nanoporous materials was subject of numerous scientific studies over the last decades. A breakthrough in the measurement of the key quantities of mass transfer was attained by the introduction of interference microscopy (IFM) [5–9]. As a consequence, the microscopic observation of intra-crystalline transient concentration profiles of the guest molecules during molecular uptake and release has become possible [10] which, moreover, can be exploited for a direct determination of intra-crystalline fluxes [11].

Conventional (macroscopic) measurements of mass transfer in nanoporous host materials record the total amount of guest molecules entering or leaving these materials during molecular uptake and release, as a function of time [1, 4, 12]. In this case, predictions on the nature of the elementary processes of mass transfer can only be based on model assumptions about the rate-limiting processes. The justification of these assumptions is a challenging task. It includes extensive measurements in which, by varying key parameters of the experiment like the size of the host crystals and/or their total amount and arrangement, the experimental results must be shown to agree with the model-based predictions [13].

Allowing the space-resolved observation of the evolution of intracrystalline concentration, micro-imaging by interference microscopy is free from these limitations. By directly following mass transfer, micro-imaging is able to correlate diffusion fluxes with the associated structural features, including the influence of the diffusion resistance of the genuine intracrystalline pore space as well as of additional resistances on the crystal boundary (the so-called surface barriers) or in the intracrystalline bulk phase.

Micro-imaging by interference microscopy is based on the measurement of the optical path length determined by a light beam passing the crystal under study [7–9]. As a con-

[1]Dr. Florian Hibbe, Dr. Christian Chmelik (chmelik@physik.uni-leipzig.de), Prof. Jörg Kärger, University of Leipzig, Faculty of Physics and Geosciences, Linnéstraße 5, 04103 Leipzig, Germany; [2]Dr. Jasper M. van Baten, Prof. Rajamani Krishna, Van 't Hoff Institute for Molecular Sciences, University of Amsterdam, Science Park 904, 1098 XH Amsterdam, The Netherlands; [3]Prof. Jens Weitkamp, University of Stuttgart, Institute of Chemical Technology, 70550 Stuttgart, Germany.

sequence, the quantity directly accessible is the integral of the concentrations in observation direction rather than the local concentration itself. Host materials with pores extended in one or two dimensions are therefore particularly convenient for this type of measurement. By choosing the observation direction perpendicular to the pore system, guest concentration in observation direction remains constant so that the concentration integral simply becomes the product of the local concentration in the given point of observation with the crystal thickness.

In this respect, zeolites of type ferrierite (FER) provide particularly favorable properties for diffusion studies by interference microscopy. They are traversed by a two-dimensional network of mutually intersecting channels with elliptical cross-sections of 4.2 Å × 5.4 Å (10-ring channels) and 3.5 Å × 4.8 Å (8-ring channels) [14] and can be synthesized in the shape of thin platelets with the channel system extended in the plane of the platelets [15, 16]. FER zeolite has thus become an ideal model system for fundamental studies of mass transfer in nanoporous materials, including the exploration of structure-mobility correlations in the crystal bulk phase [7, 17, 18] and on the crystal surface [19]. In addition, FER-type materials are also of substantial interest from a technological point of view. This results in particular from the performance of protonated ferrierite (H-FER) in the process of skeletal isomerisation of *n*-butenes towards *iso*-butene, a reactant in the production of branched ethers as important additives in lead-free gasoline with increased octane numbers and reduced pollutants emission [20 – 23].

As soon as the mass transfer in nanoporous materials may be shown to occur under ideal structural conditions, in particular under diffusion control by the genuine intracrystalline pore system, overall uptake is sufficient to provide unequivocal evidence on intracrystalline diffusion. Examples of such studies include conventional (macroscopic) uptake measurements with beds of crystallites with varying diameters [24, 25] as well as micro-imaging experiments where IR microscopy has been applied in the integral mode for covering the total uptake by an individual crystal after – by exploiting a focal plane array detector for spatially resolved measurements – diffusion limitation has been confirmed [26].

In host materials deviating from structural ideality, however, the relevant mechanisms of mass transfer cannot be revealed anymore by uptake measurement. Notably owing to Caro's work [27 – 29], mass transfer in nanoporous materials is today known to be quite commonly controlled by structural deficiencies rather than by a genuine pore space. The present communication deals with diffusion measurements in a FER crystal where the structural deficiency appears in a pronounced asymmetry of the transient concentration profiles of the guest molecules. It shall be demonstrated that even under such complicated conditions the application of interference microscopy is able to provide direct and unequivocal information about the intracrystalline diffusivities and their loading and temperature dependences as well as about the distinct mass transfer resistances on the crystal surface.

2 Methods and Material

The measurements were performed using a JENAPOL interference microscope with an interferometer of Mach-Zehnder type. By splitting, shifting and superimposing the image, this type of interferometer is able to record the difference in the optical path lengths through the crystal and the surroundings [30]. Since molecular concentration in the gas phase is negligibly small in comparison with the intracrystalline concentrations, changes in the difference of the optical path lengths are mainly due to changes in the intracrystalline concentration. Implying proportionality between optical density and guest concentration – as a reasonable first-order approach, confirmed, e.g., by comparison with the measurement of adsorption isotherms [8] – the interference patterns thus observed may be used to determine the integral over the guest concentration in observation direction.

For our experiments extra-large (30 µm × 200 µm × 10 µm) all-silica single crystals of FER were used which have been synthesized as described in [15]. In this synthesis, the entrances to the 10-ring channels on the outer surface are almost blocked [7, 17] – being opened only after additional washing with NaOH solution as demonstrated in [16, 18] – so that uptake is dominated by diffusion along the 8-ring channels. Therefore, and owing to the uniform thickness of the crystals in the direction of the 8-ring-channel, IFM is able to directly provide the profiles of intracrystalline concentration along the 8-ring channels. These profiles shall be shown in Fig. 2. They are the starting point for the exploration of the different mechanisms contributing to overall mass transfer.

Prior to the experiments, the crystals have been calcined and activated at 450 °C for at least 10 h under vacuum. Experiments were started by an essentially instantaneous increase of the pressure in the surrounding atmosphere from zero to a constant, final value. The evolution of the concentration profiles was followed with a spatial resolution of 0.5 µm and a temporal resolution of 15 s. Measurements have been performed at both room temperature (the only temperature considered in our previous studies [7, 17]) and elevated temperatures (323 and 353 K). In the latter case, before and during the experiment, the guest molecules and crystals were kept at identical and constant elevated temperatures, ensured by an appropriate heating of both the external reservoir of the guest molecules and the optical cell with the crystals [31].

Due to the underlying measurement principle, IFM provides quantitative information about only relative rather than absolute changes in concentration. This deficiency can be compensated by combination with the information of adsorption isotherms for the relevant temperatures and

pressures, stemming either from real experiments or theoretical estimates. In the present communication, either option is used by exploiting the results of IR microscopy measurements with the system under study [8, 32] and of Configurational Bias Monte Carlo (CBMC) simulations [33, 34].

3 Results and Discussion

Fig. 1a shows the adsorption isotherms of methanol in all-silica FER as resulting from CBMC simulations. The experimental data obtained by IR microscopy at room temperature are adjusted to the theoretical predictions. Also indicated are the concentrations which, after equilibration at the final pressure, result from the IFM measurements for the different temperatures considered. They were calibrated on the basis of the IR data for room temperature.

Fig. 2 provides an overview of the transient profiles of guest concentration along the direction of the 8-ring channels (y-direction) recorded by IFM during molecular uptake induced by the application of a guest pressure in the surrounding atmosphere at different temperatures. The guest concentrations are indicated on the basis of the calibration provided by Fig. 1a.

As a striking peculiarity of these profiles, immediately visible at a first glance, one notes the asymmetry in the concentration profiles. Another anomaly becomes evident with the presentations in Fig. 3a. It provides the data which, with the system under study and under the chosen experimental conditions, would result in conventional diffusion measurements, considering only the relative molecular uptake. It appears that, under the chosen experimental conditions, the rate of overall molecular uptake decreases rather than increases with increasing temperature. In the following, the complete information provided by IFM is analyzed in order to correlate these two remarkable observations with their microdynamic origin.

By implying an ideal, homogeneous crystal bulk phase, the evolution of the intracrystalline concentration follows Fick's 2nd law [1, 4, 12]:

$$\frac{\partial c}{\partial t} = \frac{\partial}{\partial y}\left(D\frac{\partial c}{\partial y}\right) = D\frac{\partial^2 c}{\partial y^2} + \frac{\partial D}{\partial c}\left(\frac{\partial c}{\partial y}\right)^2 \quad (1)$$

with the initial condition $c(y,\ t = 0) = 0$ and the boundary condition

$$j(y = 0,L)\ \left(\equiv -\ D\frac{\partial c}{\partial y}\right) = \alpha_{0,L}\,[c(y = 0,L) - c_{eq}] \quad (2)$$

D is the coefficient of intracrystalline transport diffusion (generally referred to as the transport diffusivity). It is, in general, a function of both temperature and concentration and is assumed to be uniform within the crystal. $\alpha_{0,L}$ denotes the surface permeability on either side of the crystal ($y = 0,\ L$). It is also a function of temperature and loading. Since the concentration range relevant for surface permeation covers a whole interval, namely from $c(y = 0,L)$ to c_{eq}, it cannot as easily as the transport diffusivity be attributed to one concentration, namely the given, local one. However, by considering a large variety of intervals $c(y = 0,L)$ to c_{eq}, it was found in [35] that the concentration dependence of the surface permeabilities can be satisfactorily taken account of by considering their dependence on the mean concentration $[c(y = 0,L)+c_{eq}]$. This simplification is adopted here. The surface permeabilities are assumed to be uniform on either side of the crystal while, in view of the asymmetry in the concentration profiles, they are clearly anticipated to be vastly different on the two crystal sides.

For determining, via Eq. (2), the surface permeabilities, it was realized that the fluxes $j(y = 0,\ L)$, i.e., the number of molecules passing the crystal surface per area and time, may be calculated by considering the area between the concentration profiles determined at two subsequent instants of time, taken from the crystal boundary to the profile minima, divided by the time interval between these two measurements. In this way, the surface permeabilities through the crystal boundary at $y = L$ were found to be reasonably well approached by assuming an exponential dependence of the form $k_0 \exp(k_1 c)$. The values of the fitting parameters k_0 and k_1 as determined for the different temperatures are summarized in Tab. 1.

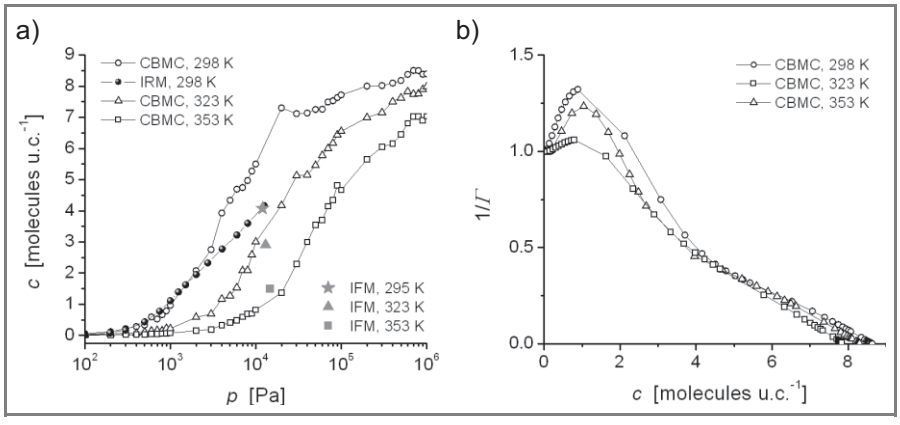

Figure 1. Equilibrium data for methanol adsorption on all-silica FER (one unit cell (u.c.) comprises two 10-ring channel segments and two cavities of 6 – 7 Å diameter, enclosed by 6- and 8-ring windows [14]). a) Adsorption isotherms determined by CBMC simulation and comparison with the experimental results obtained by IR microscopy and IFM. b) Inverse thermodynamic factor $1/\Gamma \equiv \partial \ln c/\partial \ln p$ calculated from the simulated adsorption isotherms.

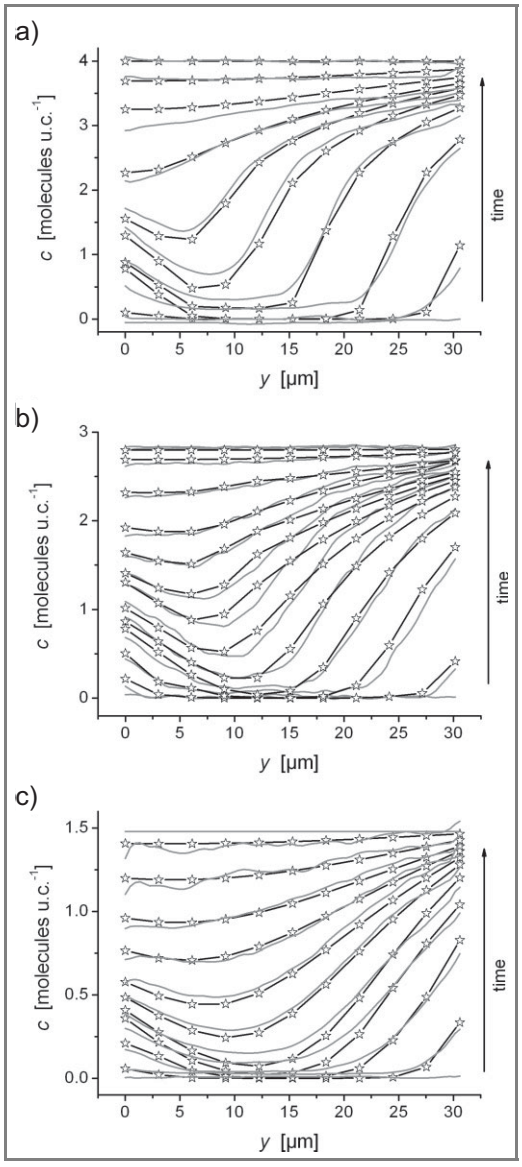

Figure 2. Transient concentration profiles of methanol in all-silica FER along the direction of the 8-ring windows (*y*-direction) induced by a pressure step in the surrounding (methanol) atmosphere from zero to 120 mbar at 295 K (a), to 130 mbar at 323 K (b) and to 145 mbar at 353 K (c). The experimental data obtained by IFM are indicated by the symbols connected with broken lines as guides for the eyes. The full lines are the respective solutions *c*(*y*,*t*) of Fick's 2nd law (Eq. (1)) subject to the boundary conditions provided by Eq. (2), with the diffusivities and surface permeabilities given in Tab. 1.

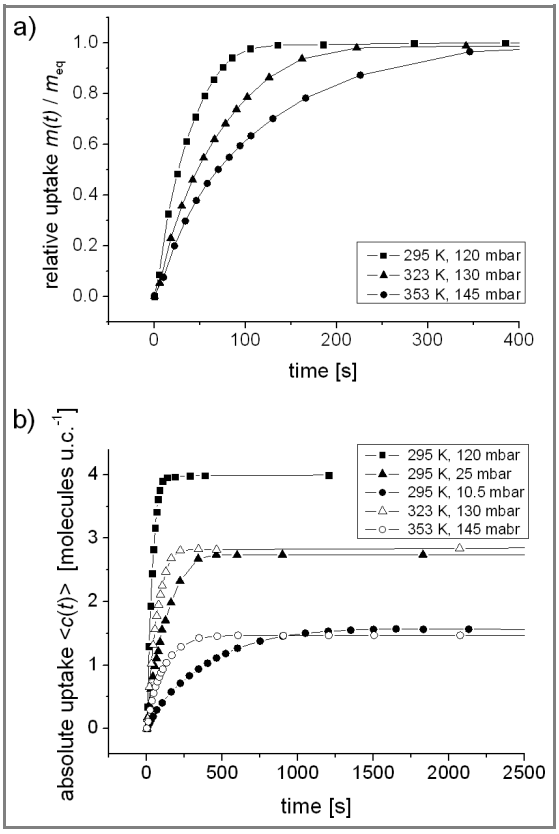

Figure 3. Time dependence of methanol uptake $m(t)$ along the 8-ring channels of all-silica FER as resulting from Fig. 2 by exploiting the relation $m(t) \propto \int_0^L c(y,t)dy$, represented a) as the relative uptake $m(t)/m_{eq}$ (with $m_{eq} = m(t\to\infty)$) and b) as the absolute uptake, in terms of the mean concentration $<c(t)> = \int_0^L c(y,t)dy/L$ with L denoting the crystal size in the direction of the 8-ring channels. Also included in b) are the results of complementary experiments at room temperature with smaller pressure steps, chosen in such a way that the resulting equilibrium concentrations m_{eq} are those of the experiments at elevated temperatures.

Table 1. Fitting parameters used for the analytic representation of the concentration dependence of the intracrystalline diffusivities (D) and of the surface permeabilities (α_L) through the crystal boundary at $y = L$ (right-hand side in the representations of Fig. 2). Both quantities could be approached by relations of the form $k_0 \exp(k_1 c)$ with the parameters k_0 and k_1 as given in the table.

	Surface permeability		Transport diffusivity	
T [K]	k_0 [10^{-8} m s^{-1}]	k_1 [(molecules per u.c.)$^{-1}$]	k_0 [10^{-13} m^{2}s^{-1}]	k_1 [(molecules per u.c.)$^{-1}$]
295	6.5	4.5	2	6.1
323	8.9	4.9	3.4	5.6
353	12.3	6	7.2	5.0

It was impossible to determine the surface permeability through the crystal boundary at $y = 0$ with a similar accuracy. The reduced permeability leads to a notably smaller flux into the crystal which results in a slower concentration increase and, hence, in a shift of the concentration minima towards $y = 0$. The area between subsequent concentration profiles and between the crystal boundary and the location of the concentration minimum on this side of the crystal could, therefore, be determined with only a very high uncertainty. Hence, via Eq. (2), also the surface permeabilities are subject to these uncertainties. However, due to the same reason, namely the notably reduced guest flow into the crystal, the surface permeabilities on this side of the crystal are

also of minor relevance for the evolution of the concentration profiles [11]. Without significant influence on the resulting concentration, the surface permeabilities on this side of the crystal can therefore be assumed to be independent of concentration. This constant value was implied to be equal to the mean value estimated via Eq. (2) for each time interval between subsequent concentration profiles for the surface permeability. The thus determined values – $\alpha_0 = 5.5$, 5.9 and $5 \cdot 10^{-8}\,m^{-1}s^{-1}$ for 295, 323 and 353 K, respectively – do not vary notably with the temperature either.

With these assumptions about the surface permeabilities and the thus specified boundary conditions, the measured concentration profiles were fitted by a finite-difference solution [36, 37] of Fick's 2nd law (Eq. (1)). It appeared that, as already with the surface permeability on the crystal side of higher permeability, the observed dependencies may be satisfactorily reproduced by assuming an exponential approach for the concentration dependencies of the diffusivities. The relevant data are summarized in Tab. 1 and the resulting concentration profiles are shown by the full lines in Fig. 2.

The asymmetry observed in the concentration profiles may thus be satisfactorily ascribed to a pronounced difference in the surface permeabilities on the two crystal faces in the entrance planes of the 8-ring channels. Simultaneously, being adequately described by a single intracrystalline diffusivity, the crystal interior is found to be completely regularly structured.

For rationalizing the deceleration of molecular uptake with increasing temperature as appearing from Fig. 3a as a second anomaly, it is refered to the representation of the surface permeabilities and intracrystalline diffusivities in Figs. 4a and b. As to be expected, for concentrations kept fixed, both the surface permeabilities and intracrystalline diffusivities clearly increase with increasing temperature. In the experiments documented in Figs. 2 and 3a, however, temperature increase is seen to be accompanied by a decrease in loading. The representations of Figs. 4a and b show that the decrease in the surface permeabilities caused by this decrease in the loadings overcompensates the effect of temperature increase, resulting in an overall decrease in both the surface permeabilities and diffusivities, i.e., in a deceleration of uptake with increasing temperature as appearing from Fig. 3a. The reasoning is supported by the representations of Fig. 3b. They show the time dependence of molecular uptake in absolute rather than relative units. In addition to the data, re-plotted from Fig. 3a, they do also include the results of uptake measurements at room temperature with notably reduced pressure steps chosen in such a way, that the final loadings did coincide with those attained with the larger pressure steps at higher temperatures. Now, in complete agreement with our expectation, uptake rates are clearly found to increase with increasing temperature.

While the mechanisms giving rise to the formation of transport resistances on the surface of nanoporous materials, being a subject of intense current discussion [31, 35, 38, 39], are still far from obvious, the transport diffusivities are well-known to be affected by two influences, which become particularly evident by using the Maxwell-Stefan notation (also referred to as the Darken equation) [4, 34, 40 – 42].

$$D = D_0\,\partial \ln p/\partial \ln c \equiv \Gamma \times D_0 \tag{3}$$

D_0 is referred to as the corrected diffusivity or, alternatively, as the Maxwell-Stefan diffusivity $Đ_{MS}$, with both notations completely equivalently in the case of single-component adsorption as considered in this study [4]. It is a measure of the translational mobility of the guest molecules and coincides with the self-diffusivity if the guest-wall interaction notably exceeds the influence of the guest-guest interaction on the molecular propagation rates – case of diverging mutual Maxwell-Stefan diffusivities $Đ_{AA}$ [34, 40, 43]. The factor $\partial \ln p/\partial \ln c$, referred to as the thermodynamic factor Γ, may be determined from the adsorption isotherm $c(p)$. Fig. 1b shows the reciprocal values ($\partial \ln c/\partial \ln p \equiv 1/\Gamma$) of the thermodynamic factors determined from the adsorption isotherms of Fig. 1a. With this representation, the decrease in loading from about 4 molecules per unit cell at 295 K to about 2.5 at 323 K and 1.5 at 353 K is seen to be accompanied by a significant increase of the thermodynamic factor and hence, with Eq. (3), by the increase of one of the factors constituting the transport diffusivities.

Fig. 4c shows the concentration dependence of the corrected (or Maxwell-Stefan) diffusivity as resulting from Eq. (3) with the thermodynamic factors given in Fig. 1b. Also here, by simultaneously increasing the temperature and decreasing the loading, the resulting corrected diffusivities are found to decrease with increasing temperature, as a consequence of the dominating influence of the loading dependence.

Starting, in the limit of vanishing concentrations, from $1/\Gamma = 1$ as for ideal systems, the reciprocal value of the thermodynamic factor in Fig. 1b is seen to increase with increasing loading. This indicates a dominance of the guest-guest interaction in comparison with the guest-host interaction which, in [44], has been referred to as the "clustering effect" and which has been described to occur, e.g., for methanol and ethanol in ZIF-8 [26], methanol in DDR and LTA [44] and alkanes in CuBTC [45, 46]. In contrast to the thermodynamic factor which for Langmuir-type isotherms is well-known to increase with increasing loading, the observed increase in the corrected diffusivities with increasing loadings is only one pattern among a multitude of concentration dependences observed for the intracrystalline mobilities. The present dependence – referred to as the type-V concentration pattern [40, 47] – may result if the activation energy for molecular propagation decreases with increasing loading [48 – 50]. Such a model is in complete agreement with the Arrhenius presentation of the corrected diffusivities in Fig. 4d, where the activation energies (slopes in the representations) decrease with increasing loading, in parallel with a significant increase in the absolute values of the diffusivities.

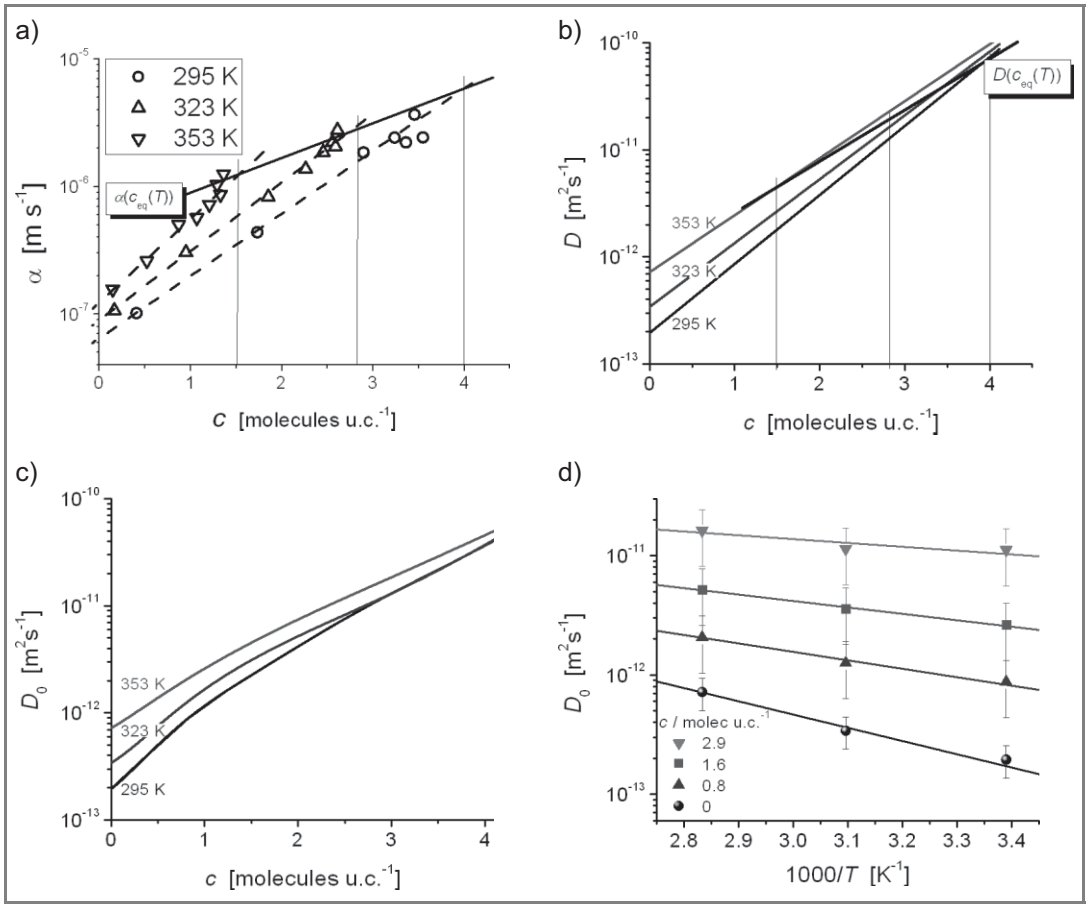

Figure 4. Surface permeability on the more permeable side (a) and intra-crystalline transport diffusivity (b) of methanol in the direction of the 8-ring channels of an all-silica crystal of type FER in dependence on the methanol concentration for the three temperatures considered in the experiments, determined with the parameters of Tab. 1. By connecting the data points to be expected for the final loadings, both the surface permeabilities and diffusivities are seen to be the smaller the larger the temperatures are. Figs. 4c and d show the corrected (or Maxwell-Stefan) diffusivities calculated via Eq. (3) with the thermodynamic factors of Fig. 1a as a function of both loading (c) and temperature (d).

4 Conclusions

Mass transfer in nanoporous materials is often influenced or even controlled by deviations from their ideal textbook structure. Under such conditions, the uptake and release rates as accessible by macroscopic techniques of diffusion measurement do scarcely provide the information necessary for identifying the rate-determining processes. As an example of such a situation, the molecular uptake by an all-silica FER crystal was considered. Zeolites of this type are known to provide particularly favorable conditions for their investigation by microscopic measurements, in particular for micro-imaging by means of interference microscopy (IFM). In this way, two remarkable findings could be attributed to their microscopic/microdynamic origin, namely (i) a pronounced asymmetry in the concentration profiles which is ascribed to notably different guest permeabilities on either side of the crystals and (ii) a slowing down of molecular uptake with increasing temperature for essentially identical pressure steps, which can be related to a dramatic concentration dependence in both the surface permeability and intracrystalline diffusivities.

Measurements of this type have only recently become possible owing to the progress in instrumentation and experiment performance, following first attempts decades ago, which have been notably promoted by Prof. Caro. With crystal sizes between tens and hundreds of micrometers, the focus of such studies is clearly not yet on materials which are scheduled for technological application. The phenomena, however, which have become accessible by direct observation, notably the transport resistances on the external surface of such materials, are known to be among the rate-determining influences in many technological applications of these materials. Their in-depth study is, correspondingly, of growing interest for both fundamental material research and a future optimized technological application of these materials.

We dedicate this paper to Professor Jürgen Caro on the occasion of his 60th birthday, in thankful recognition of a most productive cooperation over many years and of his most important contributions to the field. We are obliged to the Deutsche Forschungsgemeinschaft for financial support of the research presented in this communication.

Symbols used

a	[m s^{-1}]	Surface permeability
$a_{0,L}$	[m s^{-1}]	Surface permeability of the surface at $y=0$ or $y=L$
c	[molecules u.c.$^{-1}$]	Guest molecule concentration inside the crystal (u.c. unit cell)
c_{eq}	[molecules u.c.$^{-1}$]	Final (equilibrium) concentration of an uptake/release experiment
$<c(t)>$	[molecules u.c.$^{-1}$]	Mean concentration inside the crystal
D	[m^{2}s^{-1}]	Transport diffusivity
D_0	[m^{2}s^{-1}]	Corrected diffusivity
$Đ_{AA}$	[m^{2}s^{-1}]	Mutual Maxwell-Stefan diffusivity
$Đ_{MS}$	[m^{2}s^{-1}]	Maxwell-Stefan diffusivity
Γ	[–]	Thermodynamic factor
j	[m^{-2}s^{-1}]	Particle flux through the crystal surface
L	[m]	Crystal size in direction of the 8-ring channels
$m(t)$	[molecules m^{-3}]	Uptake at time t
m_{eq}	[molecules m^{-3}]	Uptake at equilibrium
p	[Pa]	Pressure of sorbate molecules in the surrounding atmosphere
T	[K]	Temperature
t	[s]	Time

References

[1] N. Y. Chen, T. F. Degnan, C. M. Smith, *Molecular Transport and Reaction in Zeolites*, John Wiley & Sons, New York **1994**.
[2] F. Schüth, K. S. W. Sing, J. Weitkamp, *Handbook of Porous Solids*, Wiley-VCH, Weinheim, **2002**.
[3] G. Ertl, H. Knötzinger, F. Schüth, J. Weitkamp, *Handbook of Heterogeneous Catalysis*, Wiley-VCH, Weinheim **2008**.
[4] J. Kärger, D. M. Ruthven, D. N. Theodorou, *Diffusion in Zeolites and Other Nanoporous Materials*, Wiley-VCH, Weinheim **2012**, in press.
[5] J. Kärger, R. Danz, J. Caro, *Feingerätetechnik* **1978**, *27*, 539.
[6] U. Schemmert, J. Kärger, C. Krause, R. A. Rakoczy, J. Weitkamp, *Europhys. Lett.* **1999**, *46*, 204.
[7] J. Kärger, P. Kortunov, S. Vasenkov, L. Heinke, D. B. Shah, R. A. Rakoczy, Y. Traa, J. Weitkamp, *Angew. Chem., Int. Ed.* **2006**, *45*, 7846.
[8] L. Heinke, C. Chmelik, P. Kortunov, D. M. Ruthven, D. B. Shah, S. Vasenkov, J. Kärger, *Chem. Eng. Technol.* **2007**, *30*, 995.
[9] C. Chmelik, L. Heinke, R. Valiullin, J. Kärger, *Chem. Ing. Tech.* **2010**, *82*, 779.
[10] C. Chmelik, J. Kärger, *Chem. Soc. Rev.* **2010**, *39*, 4864.
[11] L. Heinke, J. Kärger, *J. Chem. Phys.* **2009**, *130*, 044707.
[12] F. Keil, *Diffusion und Chemische Reaktion in der Gas/Feststoff-Katalyse*, Springer, Berlin **1999**.
[13] D. M. Ruthven, in *Molecular Sieves – Science and Technology: Adsorption and Diffusion* (Eds: H. G. Karge, J. Weitkamp), Springer, Berlin **2008**, 1.
[14] C. Baerlocher, L. B. McCusker, D. H. Olson, *Atlas of Zeolite Framework Types*, 6th ed., Elsevier, Amsterdam **2007**.
[15] R. A. Rakoczy, Y. Traa, P. Kortunov, S. Vasenkov, J. Kärger, J. Weitkamp, *Microporous Mesoporous Mater.* **2007**, *104*, 1195.
[16] V. R. R. Marthala, M. Hunger, F. Kettner, H. Krautscheid, C. Chmelik, J. Kärger, J. Weitkamp, *Chem. Mater.* **2011**, *23*, 2521.
[17] P. Kortunov, L. Heinke, S. Vasenkov, C. Chmelik, D. B. Shah, J. Kärger, R. A. Rakoczy, Y. Traa, J. Weitkamp, *J. Phys. Chem. B* **2006**, *110*, 23821.
[18] F. Hibbe, V. R. R. Marthala, C. Chmelik, J. Weitkamp, J. Kärger, *J. Chem. Phys.* **2011**. DOI: 10.1063/1.3652715
[19] L. Heinke, P. Kortunov, D. Tzoulaki, J. Kärger, *Phys. Rev. Lett.* **2007**, *99*, 228301.
[20] G. Onyestyak, G. Pal-Borbely, L. V. C. Rees, *Microporous Mesoporous Mater.* **2001**, *43*, 73.
[21] A. G. Stepanov, S. S. Arzumanov, M. V. Luzgin, H. Ernst, D. Freude, *J. Catal.* **2005**, *229*, 243.
[22] B. de Menorval, P. Ayrault, N. S. Gnep, M. Guisnet, *J. Catal.* **2005**, *230*, 38.
[23] S. van Donk, E. Bus, A. Broersma, J. H. Bitter, K. P. de Jong, *Appl. Catal., A* **2002**, *237*, 149.
[24] H. Yucel, D. M. Ruthven, *J. Chem. Soc. Faraday Trans. I* **1980**, *76*, 60.
[25] M. Goddard, D. M. Ruthven, *Zeolites* **1986**, *6*, 283.
[26] C. Chmelik, H. Bux, J. Caro, L. Heinke, F. Hibbe, T. Titze, J. Kärger, *Phys. Rev. Lett.* **2010**, *104*, 085902.
[27] J. Caro, M. Bülow, H. Jobic, J. Kärger, B. Zibrowius, *Adv. Catal.* **1993**, *39*, 351.
[28] J. Caro, M. Noack, F. Marlow, D. Peterson, M. Griepenstrog, J. J. Kornatowksi, *J. Phys. Chem.* **1993**, *97*, 13685.
[29] A. Feldhoff, J. Caro, H. Jobic, J. Olivier, C. B. Krause, P. Galvosas, J. Kärger, *Chem. Phys. Chem.* **2009**, *10*, 2429.
[30] U. Schemmert, J. Kärger, J. Weitkamp, *Microporous Mesoporous Mater.* **1999**, *32*, 101.
[31] F. Hibbe, C. Chmelik, L. Heinke, S. Pramanik, J. Li, D. M. Ruthven, D. Tzoulaki, J. Kaerger, *J. Am. Chem. Soc.* **2011**, *133*, 2804.
[32] H. G. Karge, J. Kärger, in *Molecular Sieves – Science and Technology: Adsorption and Diffusion* (Eds: H. G. Karge, J. Weitkamp), Springer, Berlin **2008**, 135.
[33] R. Krishna, B. Smit, S. Calero, *Chem. Soc. Rev.* **2002**, *31*, 185.
[34] R. Krishna, *J. Phys. Chem. C* **2009**, *113*, 19756.
[35] D. Tzoulaki, L. Heinke, J. Li, H. Lim, D. Olson, J. Caro, R. Krishna, C. Chmelik, J. Kärger, *Angew. Chem., Int. Ed.* **2009**, *48*, 3525
[36] L. Heinke, J. Kärger, *New J. Phys.* **2008**, *10*.
[37] M. Pernach, M. Pietrzyk, *Comp. Mater. Sci.* **2008**, *44*, 783.
[38] L. Heinke, J. Kaerger, *Phys. Rev. Lett.* **2011**, *106*.

[39] D. S. Sholl, *Nature Chemistry* **2011**, *3*, 429.
[40] F. J. Keil, R. Krishna, M. O. Coppens, *Rev. Chem. Eng.* **2000**, *16*, 71.
[41] R. Krishna, J. M. van Baten, *Microporous Mesoporous Mater.* **2008**, *109*, 91.
[42] R. Krishna, J. M. van Baten, *Chem. Eng. Sci.* **2009**, *64*, 3159.
[43] R. Krishna, D. Paschek, R. Baur, *Microporous Mesoporous Mater.* **2004**, *76*, 233.
[44] R. Krishna, J. M. van Baten, *Langmuir* **2010**, *26*, 10854.
[45] C. Chmelik, J. Kärger, M. Wiebcke, J. Caro, J. M. van Baten, R. Krishna, *Microporous Mesoporous Mater.* **2009**, *117*, 22.
[46] R. Krishna, J. M. van Baten, *Langmuir* **2010**, *26*, 8450.
[47] J. Kärger, H. Pfeifer, *Zeolites* **1987**, *7*, 90.
[48] R. Krishna, J. M. van Baten, *Microporous Mesoporous Mater.* **2009**, *125*, 126.
[49] W. Heink, J. Kärger, S. Ernst, J. Weitkamp, *Zeolites* **1994**, *14*, 320.
[50] W. Heink, J. Kärger, H. Pfeifer, K. P. Datema, A. K. Nowak, *J. Chem. Soc. Faraday Trans.* **1992**, *88*, 3505.

